

Asymmetric Transfer Hashing with Adaptive Bipartite Graph Learning

Jianglin Lu, Jie Zhou, *Member, IEEE*, Yudong Chen, Witold Pedrycz, *Life Fellow, IEEE*,
Zhihui Lai, *Member, IEEE*, Kwok-Wai Hung

Abstract—Thanks to the efficient retrieval speed and low storage consumption, learning to hash has been widely used in visual retrieval tasks. However, existing hashing methods assume that the query and retrieval samples lie in homogeneous feature space within the same domain. As a result, they cannot be directly applied to heterogeneous cross-domain retrieval. In this paper, we propose a *Generalized Image Transfer Retrieval (GITR)* problem, which encounters two crucial bottlenecks: 1) the query and retrieval samples may come from different domains, leading to an inevitable domain distribution gap; 2) the features of the two domains may be heterogeneous or misaligned, bringing up an additional feature gap. To address the GITR problem, we propose an *Asymmetric Transfer Hashing (ATH)* framework with its unsupervised/semi-supervised/supervised realizations. Specifically, ATH characterizes the domain distribution gap by the discrepancy between two asymmetric hash functions, and minimizes the feature gap with the help of a novel adaptive bipartite graph constructed on cross-domain data. By jointly optimizing asymmetric hash functions and the bipartite graph, not only can knowledge transfer be achieved but information loss caused by feature alignment can also be avoided. Meanwhile, to alleviate negative transfer, the intrinsic geometrical structure of single-domain data is preserved by involving a domain affinity graph. Extensive experiments on both single-domain and cross-domain benchmarks under different GITR subtasks indicate the superiority of our ATH method in comparison with the state-of-the-art hashing methods.

Index Terms—Adaptive bipartite graph, learning to hash, transfer learning, asymmetric hashing.

I. INTRODUCTION

DUE to the fast retrieval speed and low memory footprint, learning to hash [1]–[5] has attracted extensive attention in visual retrieval tasks over the past decades. The hashing approach aims to encode the data into compact binary codes

so as to conduct fast retrieval based on hardware-level XOR operation. Recently, a large number of hashing methods have been proposed from different perspectives [6]–[10]. However, existing hashing approaches mainly rely on two assumptions: 1) sufficient training samples are required to learn discriminative hash functions; 2) query and retrieval samples come from the same domain with the same data distribution. In real-world scenarios, these assumptions are often easily violated. Specifically, the data available in the domain of interest may be inadequate for training, leading to data sparsity problem [11]. Moreover, there may exist an inevitable data distribution discrepancy between the query and retrieval domains. To tackle these drawbacks, a feasible solution is to integrate hashing approaches with Transfer Learning (TL) [12]. TL aims to enhance the performance of target solver/learner on target domain by transferring the knowledge contained in different but related source domain [13], [14]. As a result, the dependence on sufficient target domain data can be mitigated for target solver construction.

Inspired by TL, a few number of Transfer Hashing (TH) methods have been proposed recently [11], [15]–[19]. The first TH method termed Transfer Hashing with Privileged Information (THPI) [11] marries hashing and transfer learning approaches to solve the data sparsity issue. Unlike THPI, an Optimal Projection Guided Transfer Hashing (GTH) [16] seeks for a maximum likelihood estimation solution of hash functions of target and source domains. The newly-developed Probability Weighted Compact Feature learning (PWCF) [17] provides inter-domain correlation guidance to promote cross-domain retrieval accuracy, and Discriminative Hashing Learning (DHLing) [19] constructs a domain-invariant memory bank to achieve cross-domain alignment. The above-mentioned methods, however, are all homogeneous TH methods and cannot be directly applied for heterogeneous domains. Specifically, these methods assume that target and source domains share the same feature space with the same feature dimensionality. This assumption may not always hold since the features of the two domains may be heterogeneous or misaligned. For example, the query and retrieval samples may be of different resolutions and sizes, represented by hand-crafted features with different types and lengths (e.g., color-histogram [20], SIFT [21]), or extracted by distinctive deep neural networks (e.g., VGG [22], ResNet [23]). In these cases, existing TH methods need an additional feature preprocessing (e.g. image scaling and dimension reduction) for feature alignment, which may cause information loss to a certain extent.

In this paper, we first summarize a more challenging and

Manuscript received March 14, 2022. This work was supported by the National Natural Science Foundation of China (No. 62076164), Guangdong Basic and Applied Basic Research Foundation (No. 2021A1515011861), and Shenzhen Science and Technology Program (No. JCYJ20210324094601005). (Corresponding author: Jie Zhou)

Jianglin Lu, Jie Zhou, and Zhihui Lai are with the College of Computer Science and Software Engineering, Shenzhen University, and SZU Branch, Shenzhen Institute of Artificial Intelligence and Robotics for Society, Shenzhen, Guangdong 518060, China (email: jianglinlu@outlook.com, jie_jpu@163.com, lai_zhi_hui@163.com).

Yudong Chen is with the School of Information Technology and Electrical Engineering, University of Queensland, Brisbane, QLD 4072, Australia (e-mail: yudong.chen@uq.edu.au).

Witold Pedrycz is with the Department of Electrical & Computer Engineering, University of Alberta, Edmonton, Canada, and the Systems Research Institute, Polish Academy of Sciences, Warsaw, Poland (e-mail: wpedrycz@ualberta.ca).

Kwok-Wai Hung is with Tencent Music Entertainment, Shenzhen, Guangdong 518060, China (e-mail: guoweihung@tencent.com).

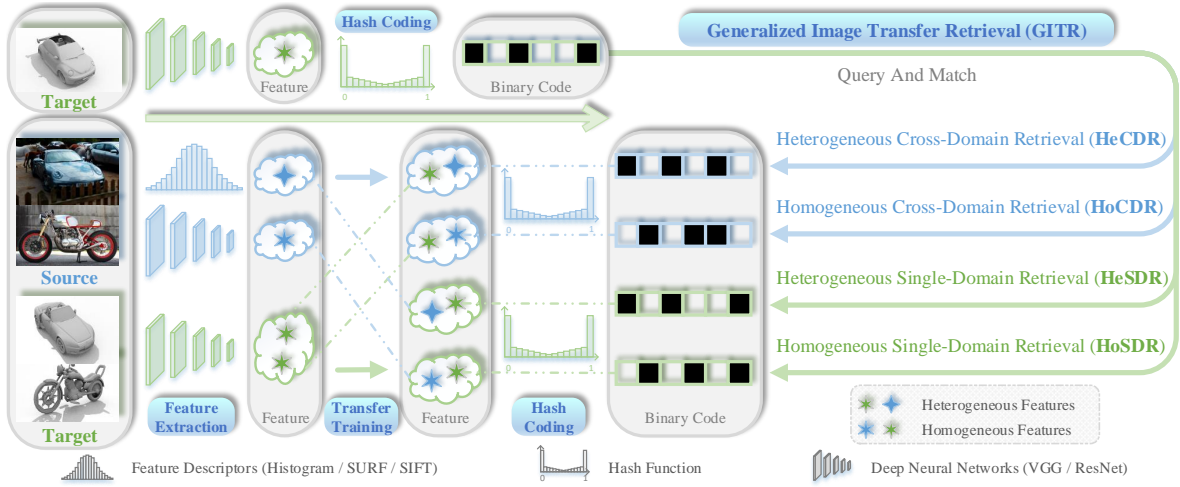


Fig. 1. Illustration of the proposed GITER problem. Without loss of generality, we assume that the query samples come from the target domain. Given a query image, heterogeneous cross-domain retrieval (HeCDR) and homogeneous cross-domain retrieval (HoCDR) aim to find the most similar samples from the source domain, while heterogeneous single-domain retrieval (HeSDR) and homogeneous single-domain retrieval (HoSDR) tend to search the ones from the target domain. Here, “He” means the features of query and retrieval sets are heterogeneous (i.e., using different feature descriptors/extractors), while “Ho” indicates homogeneous features. Best viewed in colors.

practical transfer retrieval task termed *Generalized Image Transfer Retrieval (GITER)*, in which the query and retrieval images may come from different domains and their features may be homogeneous or heterogeneous. Figure 1 gives an illustration of the proposed GITER, which contains four different subtasks, including HeCDR, HoCDR, HeSDR, and HoSDR. Without any limitation on the feature spaces and domains of query and retrieval sets, this paper aims to develop a generalized framework to solve the complicated GITER problem. Specifically, given a query image observed in \mathcal{F}_1 feature space from \mathcal{D}_1 domain, we aim to retrieve the most similar images represented in \mathcal{F}_2 feature space from \mathcal{D}_2 domain, no matter whether these two domains and two feature spaces are the same or not. To achieve this goal, we propose an *Asymmetric Transfer Hashing (ATH)* framework with its unsupervised/semi-supervised/supervised realizations. The proposed ATH contains three main components: a) asymmetric hashing learning, which characterizes domain distribution gap by the discrepancy of two asymmetric hash functions; b) cross-domain information interaction, which optimizes an adaptive bipartite graph for knowledge transfer and information fusion of cross-domain data; and c) domain structure preserving, which alleviates negative transfer by maintaining intrinsic geometrical structure of single-domain data based on domain affinity graph. The main contributions of this paper can be summarized as follows:

- We extend the current learning-to-hash problem to a more general and challenging case, dubbed GITER, which makes no assumption or restrictions on the domains and feature spaces of query and retrieval sets.
- To solve the GITER problem, we propose an ATH framework with its unsupervised/semi-supervised/supervised realizations. Specifically, ATH finds two asymmetric hash functions to encode the samples into discriminative hash codes, and learns an adaptive bipartite graph to charac-

terize the similarity between cross-domain samples.

- To our best knowledge, ATH is the first heterogeneous transfer hashing framework that jointly optimizes the asymmetric hash functions and an adaptive bipartite graph in a unified learning objective, solving the two key problems in GITER simultaneously (see Fig. 2).
- Extensive experiments conducted on both single-domain and cross-domain benchmarks indicate that existing hashing methods tailored to a special feature space and domain cannot achieve satisfactory performance, while our ATH framework can work well in different scenarios.

The rest of this paper is organized as follows. The proposed GITER problem is illustrated in Section II where we also review some related works. Section III presents the proposed ATH framework with its unsupervised/semi-supervised/supervised realizations. In Section IV, we design an iterative algorithm to optimize the objective of ATH and discuss the relationships between ATH and some related works. Section V reports on the experimental results for evaluating the performance of ATH. Conclusions and future work are covered in Section VI.

II. PRELIMINARIES

A. Generalized Image Transfer Retrieval

Suppose that we have $n = n_s + n_t$ data samples from two domains $\mathcal{D} = \{\mathcal{D}_s, \mathcal{D}_t\}$, where source domain \mathcal{D}_s and target domain \mathcal{D}_t contain n_s and n_t samples, respectively. For each domain \mathcal{D}_k , $k \in \{s, t\}$, we have $\mathcal{D}_k = \{\mathbf{X}_k, \mathbf{Y}_k\} = \{(\mathbf{x}_{k,i}, \mathbf{y}_{k,i})\}_{i=1}^{n_k}$, where $\mathbf{x}_{k,i} \in \mathbb{R}^{d_k}$ denotes the i -th sample of $\mathbf{X}_k \in \mathbb{R}^{d_k \times n_k}$ with dimensionality d_k , and $\mathbf{y}_{k,i} \in \mathbb{R}^c$ is the corresponding one-hot encoding label vector of $\mathbf{x}_{k,i}$. The hash codes of data \mathbf{X}_k are represented by $\mathbf{B}_k \in \mathbb{R}^{r \times n_k}$, where r is the length of binary codes. Moreover, \mathbf{I} , $\mathbf{1}$, and $\mathbf{0}$ denote the identity matrix, column vectors of all ones, and column vectors of all zeros with compatible size, respectively.

In the GTR problem, we do not require that the query and retrieval samples come from the same domain¹. In addition, we do not limit that the feature spaces of the two domains are homogeneous. As a result, the assumption $d_s = d_t$ existed in previous TH methods may be violated. As illustrated in Figure 1, there exists domain consistency for HeSDR and HoSDR subtasks, and domain diversity for HeCDR and HoCDR subtasks. In addition, there exists feature homogeneity for HoSDR and HoCDR subtasks, and feature heterogeneity for HeSDR and HeCDR subtasks.

B. Homogeneous Transfer Hashing

The first TH method THPI [11] incorporates privileged information from the source domain into the target domain to assist hashing learning. Its objective function can be formulated as follows:

$$\min_{\mathbf{B}_t, \mathbf{A}_t, \mathbf{A}_{sc}} \|\mathbf{E}\|^2 + \lambda_1 \|\mathbf{E} - \mathbf{A}_{sc}^T \mathbf{X}_{sc}\|^2, \quad (1)$$

$$s.t. \quad \mathbf{A}_t^T \mathbf{A}_t = \mathbf{I}, \quad \mathbf{A}_{sc}^T \mathbf{A}_{sc} = \mathbf{I},$$

where $\mathbf{E} = \mathbf{B}_t - \mathbf{A}_t^T \mathbf{X}_t$, $\mathbf{X}_{sc} \in \mathbb{R}^{d_s \times n_t}$ is n_t selected samples from source domain \mathcal{D}_s , $\mathbf{A}_t \in \mathbb{R}^{d_t \times r}$ and $\mathbf{A}_{sc} \in \mathbb{R}^{d_s \times r}$ are orthogonal projection matrices for data \mathbf{X}_t and \mathbf{X}_{sc} , respectively. As we can see, THPI utilizes data information of source domain to approximate the quantization errors of target domain. Due to $n_t \neq n_s$, THPI only uses n_t source domain samples to conduct information interaction with n_t target domain samples, which may weaken the transfer ability of target learner. In addition, how to select n_t samples from the whole source domain remains to be determined.

Unlike THPI, GTH [16] does not require to select a part of data from source domain for cross-domain information interaction. Its objective can be formulated as follows:

$$\min_{\mathbf{B}_t, \mathbf{B}_s, \mathbf{A}_t, \mathbf{A}_s} \|\mathbf{M}^{\frac{1}{2}} \odot (\mathbf{A}_t - \mathbf{A}_s)\|^2 + \lambda_1 \|\mathbf{B}_t - \mathbf{A}_t^T \mathbf{X}_t\|^2$$

$$+ \lambda_2 \|\mathbf{B}_s - \mathbf{A}_s^T \mathbf{X}_s\|^2, \quad s.t. \quad \mathbf{A}_t^T \mathbf{A}_t = \mathbf{I}, \quad \mathbf{A}_s^T \mathbf{A}_s = \mathbf{I}, \quad (2)$$

where \odot denotes element-wise product, \mathbf{M} is an error matrix derived from maximum likelihood estimation, $\mathbf{A}_s \in \mathbb{R}^{d_s \times r}$ and $\mathbf{A}_t \in \mathbb{R}^{d_t \times r}$ are hashing projections for domain \mathcal{D}_s and \mathcal{D}_t , respectively. GTH assumes that the similarity of images between target and source domains can be reversely characterized by discrepancy between hashing projections of the two domains. In other words, the weighted discrepancy between hashing projections $\mathbf{M}^{\frac{1}{2}} \odot (\mathbf{A}_t - \mathbf{A}_s)$ should be minimized to ensure that similar images from the target and source domains can be converted into similar hash codes. In this way, the whole knowledge in source domain can be used for target learner.

Instead of minimizing the discrepancy between hashing projections, PWCF [17] designs a focal-triplet loss to promote cross-domain correlations and obtains good transfer performance. Moreover, DHLing [19] further considers the problem of insufficient annotated source images and provides a

semi-supervised approach. Nevertheless, all these TH methods [11], [16]–[19] assume that the target and source domains share a homogeneous feature space with aligned features (i.e., $d_s = d_t = d$). This assumption may not always hold since the feature dimensionalities of retrieval and query samples may be misaligned. For example, the query and retrieval samples may be of distinctive resolutions and sizes, represented by hand-crafted features with different lengths, or extracted by different deep neural networks. In these cases, these methods cannot be directly applied to HeSDR and HeCDR subtasks (where $d_t \neq d_s$), which motivates us to develop a novel heterogeneous TH method to alleviate this problem.

C. Asymmetric Hashing

The earlier explorations on asymmetric hashing [24], [25] employ asymmetric distance metric for similarity preserving, where the hash codes of training and test sets are generated from the same hash function. In [26], the authors have demonstrated that using different hash functions for query and retrieval sets can achieve better approximation of target similarity with shorter code lengths. Following this work, recent asymmetric hashing methods [10], [27]–[29] tend to focus on functional space, where the distribution gap between training and test sets are characterized by the discrepancy of two distinct hash functions. In general, these methods adopt a so-called similarity-similarity difference function [1] for similarity preservation:

$$\sum_i \sum_j \|f_1(\mathbf{x}_i) f_2(\mathbf{x}_j) - r \mathbf{S}_{ij}\|^2 \quad (3)$$

where \mathbf{S} is a pre-defined label matrix, $f_1(\cdot)$ and $f_2(\cdot)$ are two distinct hash functions. Technically, they approximate the similarity between samples \mathbf{x}_i and \mathbf{x}_j as the Hamming distance between $f_1(\mathbf{x}_i)$ and $f_2(\mathbf{x}_j)$. The more similar the two samples \mathbf{x}_i and \mathbf{x}_j are, the smaller the Hamming distance between $f_1(\mathbf{x}_i)$ and $f_2(\mathbf{x}_j)$ should be. Being different from these approaches which focus on single-domain retrieval, this paper utilizes the asymmetric hashing mechanism to solve the GTR problem, especially for its challenging HeSDR and HeCDR subtasks. More importantly, since there is no label information provided for the construction of \mathbf{S} in the unsupervised scenario, we design a novel distance-similarity product function equipped with an adaptive bipartite graph to learn the potential semantic information from data.

III. METHODOLOGY

A. Graph and Bipartite Graph

Suppose that $\mathcal{G} = (\mathcal{V}, \mathcal{E}, \mathbf{W})$ is an undirected weighted graph with vertex set $\mathcal{V}(\mathcal{G})$, edge set $\mathcal{E}(\mathcal{G})$, and adjacent matrix \mathbf{W} , where each element of the real symmetric matrix \mathbf{W} measures the affinity for a pair of vertices. In general, there are three main approaches for the construction of affinity graph: 1) *nearest neighbor graph* [7], [30], [31], which focuses on local neighborhood relationship of the data; 2) *semantic graph* [32], [33], which utilizes prior semantic information of labels; 3) *adaptive graph* [34], [35], which learns adaptive graph structure from the data. On the other hand, bipartite graph

¹Note that, the definition of transfer hashing problem is different from that of cross-modal hashing. Refer to [11], [16]–[19] for more details.

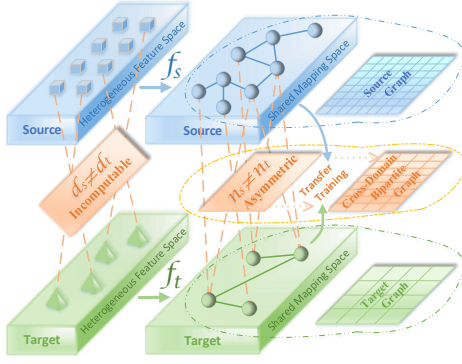


Fig. 2. Technically, the GATR faces two dilemmas: $d_s \neq d_t$ and $n_s \neq n_t$. For $d_s \neq d_t$, ATH learns two distinct hash functions f_s and f_t to transform the heterogeneous data into an alignment mapping space. For $n_s \neq n_t$, ATH optimizes an adaptive bipartite graph to integrate the whole cross-domain data for transfer training. Moreover, in order to alleviate negative transfer, ATH preserves the intrinsic geometrical structure of single-domain data by involving a domain affinity graph. Best viewed in colors.

has been extensively explored in different applications [36], [37], which can be defined as follows:

Definition 1. A graph $\mathcal{G} = (\mathcal{V}, \mathcal{E}, \mathbf{W})$ is called bipartite if $\mathcal{V} = \mathcal{V}_s \cup \mathcal{V}_t$ and $\mathcal{V}_s \cap \mathcal{V}_t = \emptyset$, such that every edge in \mathcal{E} connects one vertex from \mathcal{V}_s to one vertex from \mathcal{V}_t .

Note that, the affinity matrix $\mathbf{W} \in \mathbb{R}^{|\mathcal{V}_s| \times |\mathcal{V}_t|}$ of a bipartite graph $\mathcal{G} = (\mathcal{V}, \mathcal{E}, \mathbf{W})$ will be asymmetric if $|\mathcal{V}_s| \neq |\mathcal{V}_t|$.

B. Unsupervised ATH

Figure 2 illustrates the core idea of the proposed ATH framework, which contains three main parts including asymmetric hashing learning, cross-domain information interaction, and domain structure preserving. In this section, we first consider an unsupervised ATH (ATH_U), where neither the source domain nor the target domain contain labeled samples as the application scenarios in [11], [16].

1) *Asymmetric Hashing Learning:* In ATH, we exploit two distinct hash functions f_t and f_s to encode target and source samples separately, as follows:

$$\begin{aligned} \min_{\mathbf{B}_k, f_k} \mathcal{T}_1 &= \sum_{k \in \{s, t\}} \alpha_k \|\mathbf{B}_k - f_k(\mathbf{X}_k)\|_F^2, \\ \text{s.t. } \mathbf{B}_k &\in \{-1, 1\}^{r \times n_k}, \mathbf{B}_k \mathbf{1} = \mathbf{0}, \end{aligned} \quad (4)$$

where $\alpha_k \in \{\alpha_s, \alpha_t\}$ is a balance parameter, and $f_k \in \{f_s, f_t\}$ is the hash function of domain \mathcal{D}_k . We impose a constraint $\mathbf{B}_k \mathbf{1} = \mathbf{0}$ to make each bit to have an equal chance to be 1 or -1, thereby maintaining the most information of data. The designed optimization objective (4) aims to model the fitting error between the binary code \mathbf{B}_k and hash mapping $f_k(\mathbf{X}_k)$ for each domain \mathcal{D}_k . Note that, $f_k(\cdot)$ can be any suitable mapping function, such as linear function and kernel function. For ATH_U, we just exploit a simple yet effective linear function:

$$f_k(\mathbf{x}_{k,i}) = \mathbf{A}_k^T \mathbf{x}_{k,i}, \quad (5)$$

where $\mathbf{A}_k \in \{\mathbf{A}_s, \mathbf{A}_t\}$ is a hashing projection. Most notably, $\mathbf{A}_s \in \mathbb{R}^{d_s \times r}$ and $\mathbf{A}_t \in \mathbb{R}^{d_t \times r}$ can be of the same magnitude

or not. If $d_s = d_t$, it can be used for HoSDR and HoCDR. Otherwise, it is tailored to HeSDR and HeCDR.

2) *Cross-Domain Information Interaction:* We consider conducting direct knowledge transfer and fusion between target and source domains, regardless of whether these two domains share the same feature space or not. Obviously, it is infeasible to minimize the errors between \mathbf{A}_s and \mathbf{A}_t as in [16] since the cross-domain features may be misaligned. According to Definition 1, we observe that if we regard the source and target data as a whole dataset, on which we can naturally construct a bipartite graph $\mathcal{G}_{st} = (\mathcal{V}_{st}, \mathcal{E}_{st}, \mathbf{W}_{st})$ where $\mathcal{V}_{st} = \mathbf{X}_s \cup \mathbf{X}_t$ and $\mathbf{W}_{st} \in \mathbb{R}^{n_s \times n_t}$. Nevertheless, how to determine the edge set \mathcal{E}_{st} and edge weight \mathbf{W}_{st} becomes a knotty problem. Note that, we cannot apply a nearest neighbor bipartite graph in HeSDR and HeCDR subtasks since the distances between heterogeneous features of cross-domain data cannot be calculated directly, as shown in Figure 2. To mitigate this problem, we propose to learn an adaptive bipartite graph from data to characterize the affinities of cross-domain samples, by the following distance-similarity product function:

$$\begin{aligned} \min_{\mathbf{W}_{st}, f_k} \mathcal{T}_2 &= \lambda \sum_{i=1}^{n_s} \sum_{j=1}^{n_t} \mathbf{F}_{st,ij} \mathbf{W}_{st,ij} + \gamma \|\mathbf{W}_{st}\|_F^2, \\ \text{s.t. } \forall_i, \quad \mathbf{W}_{st,i} &\geq \mathbf{0}, \quad \mathbf{W}_{st,i}^T \mathbf{1} = 1 \end{aligned} \quad (6)$$

where λ and γ are two hyper-parameters, $\mathbf{W}_{st,i}$ is the i -th row of \mathbf{W}_{st} , and $\mathbf{F}_{st,ij} = \|f_s(\mathbf{x}_{s,i}) - f_t(\mathbf{x}_{t,j})\|^2$ models the distances (or fitting errors) between hash mappings of cross-domain samples. The value of $\mathbf{W}_{st,ij}$ can be viewed as the probability that two cross-domain samples $\mathbf{x}_{s,i}$ and $\mathbf{x}_{t,j}$ belong to the same class. Therefore, we make the constraint $\mathbf{W}_{st,i} \geq \mathbf{0}$. In addition, the constraint $\mathbf{W}_{st,i}^T \mathbf{1} = 1$ is imposed to avoid a trivial case where all elements of $\mathbf{W}_{st,i}$ are zero, and the regularization term $\gamma \|\mathbf{W}_{st}\|_F^2$ provide the probability prior of uniform distribution. As we can see, the designed distance-similarity product function (6) enables the solver to simultaneously learn hash functions and affinity relationship of cross-domain samples, regardless of whether the features of the two domains are misaligned or not. This optimization objective stems from a straightforward intuition that the more similar two cross-domain samples (i.e., the larger $\mathbf{W}_{st,ij}$) are, the less difference the corresponding hash mappings (i.e., the smaller $\mathbf{F}_{st,ij}$) should be. The joint optimization of asymmetric hash functions and bipartite graph promotes knowledge fusion between cross-domain data and makes it possible to conduct transfer training in heterogeneous domains.

3) *Domain Structure Preserving:* When performing transfer training, negative transfer becomes a problem worthy of careful consideration. To mitigate this problem, we preserve the intrinsic geometrical structure of single-domain data by involving a domain affinity graph. Specifically, for each domain \mathcal{D}_k , we first construct a nearest neighbor graph $\mathcal{G}_k = (\mathcal{V}_k, \mathcal{E}_k, \mathbf{W}_k)$, where $\mathcal{V}_k = \mathbf{X}_k$ and \mathcal{E}_k is defined as:

$$\mathcal{E}_k = \{ \langle \mathbf{x}_{k,i}, \mathbf{x}_{k,j} \rangle \mid i \in \mathcal{N}_{\eta_k}(j) \cup j \in \mathcal{N}_{\eta_k}(i) \} \quad (7)$$

where $\mathcal{N}_{\eta_k}(i)$ denotes the set of η_k nearest neighbors of $\mathbf{x}_{k,i}$. With the defined edge set \mathcal{E}_k , we can simply set the edge

Algorithm 1: Optimization for ATH_U

1 **Input:** Training sets $\mathbf{X}_k \in \{\mathbf{X}_s, \mathbf{X}_t\}$.
2 **Parameter:** $\alpha_k, \beta_k, \lambda, r$, maximum iterations Ite .
3 **Output:** Hashing projections $\mathbf{A}_k \in \{\mathbf{A}_s, \mathbf{A}_t\}$.
4: Construct affinity matrices $\mathbf{W}_k \in \{\mathbf{W}_s, \mathbf{W}_t\}$;
5: Initialize \mathbf{A}_k by PCA projections;
6: Initialize \mathbf{B}_k by $\mathbf{B}_k = \text{sign}(\mathbf{A}_k^T \mathbf{X}_k)$;
7: **while** converge or reach maximum iterations Ite **do**
8: Update \mathbf{A}_k according to (17);
9: Update \mathbf{M}_k by $\mathbf{M}_k = \alpha_k \mathbf{A}_k^T \mathbf{X}_k$;
10: **for** $i = 1 : r$ **do**
11: Update $\mathbf{B}_{k,ij}$ according to (19);
12: **end for**
13: Update $\mathbf{W}_{st,i}$ according to (21);
14: **end for**
15: **end while**

weight $\mathbf{W}_k \in \mathbb{R}^{n_k \times n_k}$ as follows:

$$\mathbf{W}_{k,ij} = \begin{cases} 1, & \text{if } \langle \mathbf{x}_{k,i}, \mathbf{x}_{k,j} \rangle \in \mathcal{E}_k, \\ 0, & \text{otherwise} \end{cases} \quad (8)$$

Then, we design the following optimization objective to force the similar samples of each domain to be as close as possible in the corresponding mapping space:

$$\min_{f_k} \mathcal{T}_3 = \sum_{k \in \{s,t\}} \beta_k \sum_{i=1}^{n_k} \sum_{j=1}^{n_k} \mathbf{F}_{k,ij} \mathbf{W}_{k,ij}, \quad (9)$$

where $\beta_k \in \{\beta_s, \beta_t\}$ is a balance parameter, and $\mathbf{F}_{k,ij} = \|f_k(\mathbf{x}_{k,i}) - f_k(\mathbf{x}_{k,j})\|^2$ models the fitting errors between hash mappings of single-domain samples.

4) *Overall Objective Function:* The overall objective function of the proposed ATH_U is formulated as follows:

$$\begin{aligned} \min_{\mathbf{B}_k, \mathbf{W}_{st}, f_k} \mathcal{J} &= \mathcal{T}_1 + \mathcal{T}_2 + \mathcal{T}_3 \\ \text{s.t. } \mathbf{B}_k &\in \{-1, 1\}^{r \times n_k}, \quad \mathbf{B}_k \mathbf{1} = \mathbf{0}, \\ \forall i, \quad \mathbf{W}_{st,i} &\geq 0, \quad \mathbf{W}_{st,i}^T \mathbf{1} = 1 \end{aligned} \quad (10)$$

The joint objective function (10) can be optimized by a well-designed iterative algorithm, as shown in Section IV-A.

C. Semi-supervised ATH

This section provides a semi-supervised realization of ATH termed ATH_M, where all samples in the source domain are well annotated as the application scenarios in [17], [19]. The difference of objective functions between ATH_U and ATH_M lies in the construction of source graph. Unlike ATH_U, ATH_M adopts a semantic graph for the source domain. Specifically, ATH_M defines the edge set \mathcal{E}_s of source graph $\mathcal{G}_s = (\mathcal{X}_s, \mathcal{E}_s, \mathbf{W}_s)$ as follows:

$$\mathcal{E}_s = \{\langle \mathbf{x}_{s,i}, \mathbf{x}_{s,j} \rangle \mid \mathbf{y}_{s,i} = \mathbf{y}_{s,j}\} \quad (11)$$

The edge weight setting of ATH_M is similar to that of ATH_U. As can be seen from Eq. 11, ATH_M exploits semantic information of the source domain to perform transfer training, which promotes the performance of hash encoders.

D. Supervised ATH and Kernel Extension

This section presents a supervised realization of ATH dubbed ATH_S, which is tailored to the case where all samples in the source and target domains are well labeled. With the available label information, we do not need to optimize an adaptive bipartite graph for cross-domain knowledge transfer as in Eq. 6. Instead, ATH_S proactively constructs a semantic bipartite graph and sets its edge set \mathcal{E}_{st} as:

$$\mathcal{E}_{st} = \{\langle \mathbf{x}_{s,i}, \mathbf{x}_{t,j} \rangle \mid \mathbf{y}_{s,i} = \mathbf{y}_{t,j}\} \quad (12)$$

In this way, semantic similarity of cross-domain data can be used to conduct domain alignment and improve the transferability of our model. As for the source and target graphs $\mathcal{G}_k = (\mathbf{X}_k, \mathcal{E}_k, \mathbf{W}_k)$, we also utilize semantic information to construct the edge set \mathcal{E}_k for each domain \mathcal{D}_k as follows:

$$\mathcal{E}_k = \{\langle \mathbf{x}_{k,i}, \mathbf{x}_{k,j} \rangle \mid \mathbf{y}_{k,i} = \mathbf{y}_{k,j}\} \quad (13)$$

As mentioned in Eq. 4, we can use a kernel function for realizing f_k . To explore the performance of kernel function, we further present a kernel extension of ATH_S named ATH_K, of which the hash function can be formulated as:

$$\hat{f}_k(\mathbf{x}_{k,i}) = \mathbf{A}_k^T \phi(\mathbf{x}_{k,i}), \quad (14)$$

where $\phi(\mathbf{x}_{k,i})$ is a $m_k \in \{m_s, m_t\}$ -dimensional column vector obtained by Gaussian kernel

$$\phi(\mathbf{x}_{k,i}) = \left[\exp\left(-\frac{\|\mathbf{x}_{k,i} - \chi_{k,1}\|^2}{\sigma}\right), \dots, \exp\left(-\frac{\|\mathbf{x}_{k,i} - \chi_{k,m_k}\|^2}{\sigma}\right) \right]^T \quad (15)$$

where $\{\chi_{k,j}\}_{j=1}^{m_k}$ are m_k anchor points randomly selected from domain \mathcal{D}_k , and σ is the kernel width [38].

IV. DISCUSSION

A. Optimization

Due to space limitation, we only provide the optimization algorithm for ATH_U. The optimization approaches of ATH_M, ATH_S, and ATH_K are similar to that of ATH_U. Specifically, our iterative algorithm updates one variable at a time by fixing the others, as listed in Algorithm 1.

A_k-Step. The subproblem of $\mathbf{A}_k \in \{\mathbf{A}_s, \mathbf{A}_t\}$ is equal to the following unconstrained minimization problem:

$$\begin{aligned} \min_{\mathbf{A}_k} \quad & \alpha_k \|\mathbf{B}_k - \mathbf{A}_k^T \mathbf{X}_k\|_F^2 + \beta_k \text{tr}(\mathbf{A}_k^T \mathbf{X}_k \mathbf{L}_k \mathbf{X}_k^T \mathbf{A}_k) \\ & + \lambda \text{tr}(-2\mathbf{A}_k^T \mathbf{X}_k \tilde{\mathbf{W}}_{st} \tilde{\mathbf{X}}_k^T \tilde{\mathbf{A}}_k + \mathbf{A}_k^T \mathbf{X}_k \tilde{\mathbf{D}}_{st} \mathbf{X}_k^T \mathbf{A}_k) \\ = \quad & \text{tr}(\mathbf{A}_k^T (\mathbf{X}_k (\alpha_k \mathbf{I} + \beta_k \mathbf{L}_k + \lambda \tilde{\mathbf{D}}_{st}) \mathbf{X}_k^T) \mathbf{A}_k \\ & - 2\mathbf{A}_k^T \mathbf{X}_k (\alpha_k \mathbf{B}_k^T + \lambda \tilde{\mathbf{W}}_{st} \tilde{\mathbf{X}}_k^T \tilde{\mathbf{A}}_k)), \end{aligned} \quad (16)$$

where $\tilde{\mathbf{D}}_{st} \in \mathbb{R}^{n_k \times n_k}$ is a diagonal matrix, $\mathbf{L}_k \in \{\mathbf{L}_s, \mathbf{L}_t\}$ is the graph Laplacian matrix, $\mathbf{L}_k = \mathbf{D}_k - \mathbf{W}_k$, and $\mathbf{D}_k \in \mathbb{R}^{n_k \times n_k}$ is a diagonal matrix with $\mathbf{D}_{k,ii} = \sum_j \mathbf{W}_{k,ij}$. In (16), if $k = s$, $\tilde{\mathbf{D}}_{st,ii} = \sum_j \mathbf{W}_{st,ij}$, $\tilde{\mathbf{W}}_{st} = \mathbf{W}_{st}$, $\tilde{\mathbf{X}}_k = \mathbf{X}_t$, and $\tilde{\mathbf{A}}_k = \mathbf{A}_t$. Otherwise, $\tilde{\mathbf{D}}_{st,jj} = \sum_i \mathbf{W}_{st,ij}$, $\tilde{\mathbf{W}}_{st} = \mathbf{W}_{st}^T$, $\tilde{\mathbf{X}}_k = \mathbf{X}_s$, and $\tilde{\mathbf{A}}_k = \mathbf{A}_s$. By setting the derivative of

(16) with respect to \mathbf{A}_k to zero, the optimal solution of \mathbf{A}_k subproblem can be obtained by²:

$$\mathbf{A}_k = \Phi_k^{-1}(\alpha_k \mathbf{X}_k \mathbf{B}_k^T + \lambda \mathbf{X}_k \widetilde{\mathbf{W}}_{st} \widetilde{\mathbf{X}}_k^T \widetilde{\mathbf{A}}_k), \quad (17)$$

where $\Phi_k = \mathbf{X}_k(\alpha_k \mathbf{I}_{n_k} + \beta_k \mathbf{L}_k + \lambda \mathbf{I}_{n_k}) \mathbf{X}_k^T$.

B_k-Step. The subproblem of $\mathbf{B}_k \in \{\mathbf{B}_s, \mathbf{B}_t\}$ is equal to the following non-convex problem with discrete constraints:

$$\max_{\mathbf{B}_k \in \{-1, 1\}^{r \times n_k}, \mathbf{B}_k \mathbf{1} = \mathbf{0}} \text{tr}(\mathbf{B}_k^T \mathbf{M}_k), \quad (18)$$

where $\mathbf{M}_k = \alpha_k \mathbf{A}_k^T \mathbf{X}_k$. The optimal solution of this maximization problem can be directly obtained by sorting the elements of each row of \mathbf{M}_k :

$$\mathbf{B}_{k,ij} = \begin{cases} 1, & \text{if } j \in \tau(i), \\ -1, & \text{otherwise} \end{cases} \quad (19)$$

where $\tau(i)$ indicates an index set of the first $n_k/2$ maximal elements of $\mathbf{M}_{k,i}$, and $\mathbf{M}_{k,i}$ indicates the i -th row of \mathbf{M}_k .

W_{st}-Step. To solve the subproblem of \mathbf{W}_{st} , we need to address n_s decoupled independent problems as follows:

$$\begin{aligned} \min_{\mathbf{W}_{st,i}} & \|\mathbf{W}_{st,i} + \frac{\lambda}{2\gamma_i} \mathbf{F}_{st,i}\|^2, \\ \text{s.t.} & \mathbf{W}_{st,i} \geq 0, \quad \mathbf{W}_{st,i}^T \mathbf{1} = 1 \end{aligned} \quad (20)$$

For problem (20), we have the following theorem:

Theorem 1. Let the number of nonzero elements in $\mathbf{W}_{st,i}$ be $\eta \in \{1, \dots, n_t\}$. Then the optimal solution of (20) is:

$$\mathbf{W}_{st,i} = \left(\frac{1 + \sum_{j=1}^{\eta} \frac{\lambda}{2\gamma_i} \widetilde{\mathbf{F}}_{st,ij}}{\eta} \mathbf{1} - \frac{\lambda}{2\gamma_i} \mathbf{F}_{st,i} \right)_+ \quad (21)$$

where the operator $(\cdot)_+$ turns the negative elements to zero while keeps the rest, and the elements of $\widetilde{\mathbf{F}}_{st,i}$ are those of $\mathbf{F}_{st,i}$ but with the ascending order.

Proof. The Lagrangian function of the \mathbf{W}_{st} subproblem can be formulated as follows:

$$\mathcal{L} = \frac{1}{2} \|\mathbf{W}_{st,i} + \frac{\lambda}{2\gamma_i} \mathbf{F}_{st,i}\|^2 - \varphi(\mathbf{W}_{st,i}^T \mathbf{1} - 1) - \mathbf{u}^T \mathbf{W}_{st,i}, \quad (22)$$

where φ and \mathbf{u} are Lagrangian multipliers. By taking the derivate of \mathcal{L} with respect to $\mathbf{W}_{st,i}$ and setting it zero, with the KKT condition, we obtain:

$$\begin{aligned} \frac{\partial \mathcal{L}}{\partial \mathbf{W}_{st,i}} &= \mathbf{W}_{st,i} + \frac{\lambda}{2\gamma_i} \mathbf{F}_{st,i} - \varphi \mathbf{1} - \mathbf{u} = 0; \\ \mathbf{W}_{st,i}^T \mathbf{1} - 1 &= 0; \quad \mathbf{u}^T \mathbf{W}_{st,i} = 0 \end{aligned} \quad (23)$$

For the third equation, if $\mathbf{W}_{st,ij} > 0$, then we have $\mathbf{u}_j = 0$. Therefore, the solution of $\mathbf{W}_{st,i}$ is:

$$\mathbf{W}_{st,i} = \left(\varphi \mathbf{1} - \frac{\lambda}{2\gamma_i} \mathbf{F}_{st,i} \right)_+ \quad (24)$$

Since $\mathbf{W}_{st,i}$ has η nonzero elements and $\mathbf{W}_{st,i} \geq 0$, we have:

$$\varphi - \frac{\lambda}{2\gamma_i} \widetilde{\mathbf{F}}_{st,i\eta} > 0 \quad \cap \quad \varphi - \frac{\lambda}{2\gamma_i} \widetilde{\mathbf{F}}_{st,i(\eta+1)} \leq 0 \quad (25)$$

²In practice, we generally add a regularization as $\widetilde{\Phi}_k = \Phi_k + \varphi \mathbf{I}$ ($\varphi > 0$) to solve the singularity problem if it exists.

According to $\mathbf{W}_{st,i}^T \mathbf{1} = 1$ and Eq. 24, we obtain:

$$\sum_{j=1}^{\eta} \left(\varphi - \frac{\lambda}{2\gamma_i} \widetilde{\mathbf{F}}_{st,ij} \right) = 1 \Rightarrow \varphi = \frac{1 + \sum_{j=1}^{\eta} \frac{\lambda}{2\gamma_i} \widetilde{\mathbf{F}}_{st,ij}}{\eta} \quad (26)$$

Substitute Eq. 26 into Eq. 24, and we can obtain the same solution as stated in Theorem 1. \square

B. Parameter Setting of γ

In this section, we show how to determine the value of parameter γ . Combining Eq. 25 and 26, we can obtain:

$$\frac{\lambda\eta}{2} \widetilde{\mathbf{F}}_{st,i\eta} - \frac{\lambda}{2} \sum_{j=1}^{\eta} \widetilde{\mathbf{F}}_{st,ij} < \gamma_i \leq \frac{\lambda\eta}{2} \widetilde{\mathbf{F}}_{st,i(\eta+1)} - \frac{\lambda}{2} \sum_{j=1}^{\eta} \widetilde{\mathbf{F}}_{st,ij} \quad (27)$$

In order to make the optimal solution of $\mathbf{W}_{st,i}$ have η nonzero values, we can set γ_i as:

$$\gamma_i = \frac{\lambda\eta}{2} \widetilde{\mathbf{F}}_{st,i(\eta+1)} - \frac{\lambda}{2} \sum_{j=1}^{\eta} \widetilde{\mathbf{F}}_{st,ij} \quad (28)$$

As a result, we do not need to turn the value of parameter γ . We can set its value as the average of γ_i for $i \in \{1, 2, \dots, n_s\}$:

$$\gamma = \frac{1}{n_s} \sum_{i=1}^{n_s} \left(\frac{\lambda\eta}{2} \widetilde{\mathbf{F}}_{st,i(\eta+1)} - \frac{\lambda}{2} \sum_{j=1}^{\eta} \widetilde{\mathbf{F}}_{st,ij} \right) \quad (29)$$

C. Connections to Previous Methods

We analyze the connections and differences between the proposed ATH and some related hashing methods, including anchor-graph-based hashing [6], [39], [40], asymmetric hashing [10], [27], [29], and transfer hashing [11], [16], [17], [19].

The anchor-graph-based hashing methods [6], [39], [40] aim to perform fast graph construction for large-scale image retrieval. In fact, anchor graph can be viewed as a special bipartite graph. Unlike these methods focusing on single-domain image retrieval, we utilize the bipartite graph to integrate cross-domain information for transfer hashing. Moreover, these methods are all two-step approaches, which first pre-construct an anchor graph through clustering and then use it to learn hash functions. Nevertheless, our proposed ATH can learn the bipartite graph and hash functions simultaneously in a unified framework.

The asymmetric hashing methods [10], [27], [29] emphasize achieving similarity approximation with short binary codes. To achieve this goal, they usually adopt the so-called similarity-similarity difference function [1] for similarity preservation. Unlike these approaches, the proposed ATH aims to learn distinguish hash functions with unaligned inputs for the source and target domains by incorporating the asymmetric hashing mechanism. Therefore, ATH can solve the transfer hashing problem, especially for the HeCDR task with misaligned features. Moreover, ATH constructs a distance-similarity product function [1] for similarity preserving, which helps to jointly optimize the bipartite graph and hash functions.

The transfer hashing methods [16], [17], [19] are proposed to deal with cross-domain retrieval task. These methods find

TABLE I
MAP (%) RESULTS OF DIFFERENT METHODS WITH VARYING CODE LENGTHS FROM 16 TO 128 ON SINGLE-DOMAIN DATASETS.

Method	16	32	48	64	96	128	16	32	48	64	96	128
	SUN397 {train 106,953:test 1,800}						CIFAR-10 {train 59,000:test 1,000}					
ITQ	7.25	9.57	10.07	10.69	12.33	12.70	15.22	15.97	16.10	16.21	16.72	16.88
SP	8.68	10.55	11.60	12.98	14.14	14.74	16.23	16.51	16.98	17.20	17.61	17.85
DPLM	11.11	13.71	16.49	17.81	19.35	19.88	16.83	18.31	19.32	19.50	20.13	20.17
SHSR	12.40	16.31	18.03	16.76	18.01	17.87	17.35	17.05	16.85	16.47	15.75	15.36
GTH	8.04	11.31	12.93	13.51	14.41	15.36	15.07	16.23	16.53	16.77	17.12	16.40
ATH_U	13.87	17.47	19.14	19.89	22.09	22.90	18.01	19.54	20.69	20.82	20.91	21.02

TABLE II
MAP (%) RESULTS OF DIFFERENT METHODS WITH VARYING CODE LENGTHS FROM 16 TO 128 ON THE HoSDR SUBTASK.

Method	16	32	48	64	96	128	16	32	48	64	96	128	16	32	48	64	96	128
	P → A						R → C						P → C					
ITQ	14.40	25.21	28.25	30.88	33.38	34.21	8.36	12.41	14.81	16.24	17.74	18.46	8.18	12.34	14.34	15.39	17.05	17.54
SP	18.10	32.82	37.11	38.33	39.99	40.22	9.62	14.81	17.37	18.51	19.68	20.22	9.26	14.17	16.57	17.60	18.75	19.41
DPLM	24.54	36.10	40.52	42.73	47.06	47.41	11.51	16.39	18.21	19.47	21.39	21.77	11.92	15.35	16.88	17.77	19.85	20.59
SHSR	19.23	35.56	38.73	39.50	41.60	41.43	10.14	16.01	18.05	18.99	19.60	19.66	9.30	14.33	17.03	18.09	18.22	18.13
GTH	17.48	25.81	28.61	31.62	33.98	33.96	8.59	13.05	15.95	17.14	18.73	19.53	8.47	12.78	15.13	16.49	17.88	18.39
ATH_U	37.86	46.54	48.50	48.65	48.70	48.43	17.40	23.81	24.96	25.76	24.88	24.97	15.99	21.79	22.89	23.82	23.61	24.07

TABLE III
MAP (%) RESULTS OF DIFFERENT METHODS WITH VARYING CODE LENGTHS FROM 16 TO 128 ON THE HoCDR SUBTASK.

Method	16	32	48	64	96	128	16	32	48	64	96	128	16	32	48	64	96	128
	C → A						A → P						C → P					
ITQ	6.16	10.03	12.07	13.16	14.09	14.89	11.85	17.37	20.11	21.63	22.90	23.14	10.58	15.46	18.37	19.54	20.61	21.31
SP	7.49	14.04	16.07	17.09	17.72	17.98	16.06	24.67	26.86	27.79	28.55	28.33	13.13	19.89	22.89	23.94	24.79	24.92
DPLM	10.53	15.76	18.68	19.94	21.95	22.00	18.35	26.22	29.56	32.61	34.13	35.48	17.14	24.51	26.74	28.54	29.23	30.34
SHSR	13.22	17.87	18.68	18.60	18.35	16.55	17.67	27.75	27.17	28.13	26.24	24.30	15.73	24.99	26.54	26.99	25.36	23.72
GTH	7.15	10.09	12.08	13.06	14.51	14.88	10.91	17.44	20.46	21.42	22.50	22.91	10.93	16.48	18.34	18.69	19.24	19.55
ATH_U	17.00	23.76	25.68	27.05	27.21	26.49	24.03	32.03	33.45	34.15	34.85	34.14	20.64	27.13	28.49	29.81	29.72	29.87

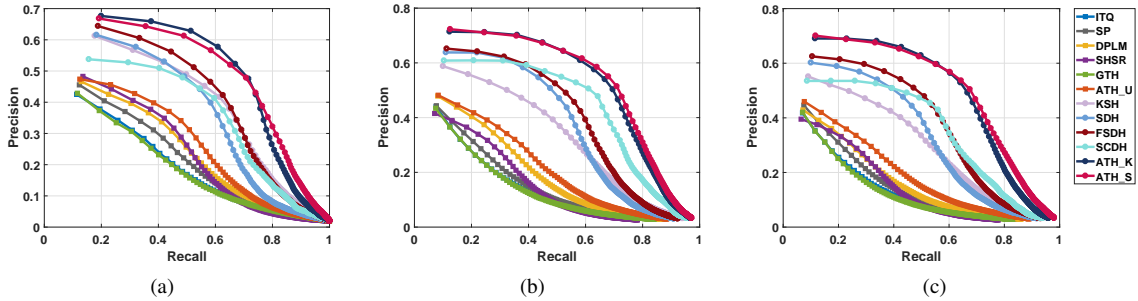


Fig. 3. PR curves on the HoSDR subtask. (a) P → A, (b) R → C, (c) P → C.

either a shared hash function or two different hash functions with aligned inputs for source and target domains. As a result, they cannot be directly applied in HeSDR and HeCDR tasks, since the feature dimensionalities of source and target domains in these two tasks are inconsistent. The proposed ATH can handle this problem by learning asymmetric hash functions. Moreover, the transfer hashing method [11] need to select a part of source samples to integrate information with the target samples, while our ATH can perform cross-domain information interaction for all source and target sample through the learning of a bipartite graph.

D. Time Complexity

As listed in Algorithm 1, the main computation burden of ATH_U comes from iteratively updating \mathbf{A}_k , \mathbf{B}_k , and \mathbf{W}_{st} . The main computation cost for optimizing \mathbf{A}_k and \mathbf{B}_k are $\mathcal{O}(d_k^3)$ and $\mathcal{O}(rn_k \log n_k)$ respectively. And we need

$\mathcal{O}(n_s n_t \log n_t)$ for the optimization of \mathbf{W}_{st} . In transfer hashing task, there usually exists $n_t \ll n_s$. Therefore, the computation cost of our algorithm is acceptable.

V. EXPERIMENTS

In our experiments, we compare the proposed ATH_U with unsupervised hashing methods ITQ [41], SP [42], DPLM [43], SHSR [44], and transfer hashing method GTH [16]. For ATH_K and ATH_S, we compare them with supervised hashing methods KSH [45], SDH [38], FSDH [46], and SCDH [47]. For ATH_M, we compare it with KSH, SDH and transfer hashing methods PWCF [17] and DHLing [19].

A. Datasets

To evaluate the performance of our ATH framework, we conduct experiments both on the single-domain and cross-domain datasets. The used datasets are described as follows:

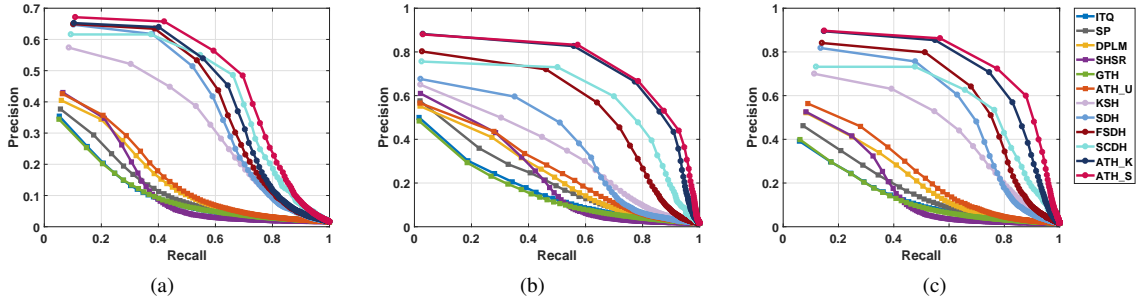


Fig. 4. PR curves on the HoCDR subtask. (a) $C \rightarrow A$, (b) $A \rightarrow P$, (c) $C \rightarrow P$.

1) *Single-domain Datasets*: We first evaluate the proposed ATH_U on single-domain datasets, including CIFAR-10³ and SUN397 [48] datasets. The CIFAR-10 dataset contains 60,000 images of 10 classes, where 59,000 images (5,900 images sampled from each class) are randomly selected for training and the rest images are used for testing. The SUN397 dataset includes 108,753 scene images from 397 well-sampled categories, where each category contains at least 100 samples. In our experiments, the training set contains 106,953 images and the rest 1,800 images are used for testing.

2) *Cross-domain Datasets*: For the proposed GTR task, we test our ATH framework on three cross-domain benchmarks, including Office Home [49], Caltech&Amazon [50] and VisDA [51]. Specifically, for HoSDR and HoCDR subtasks, we follow [17], [19] and conduct experiments on Office Home, which is a well-known cross-domain benchmark containing four different domains: Artistic (A), Clip Art (C), Product (P), and Real-World (R). For simplicity, we use $\# \rightarrow \&$ to indicate that the source domain is $\#$ and the target domain is $\&$. For HeSDR and HeCDR subtasks, we conduct experiments on Caltech&Amazon and VisDA benchmarks. Caltech&Amazon is constructed from Office-Caltech10 dataset [50], which includes images of 10 classes from different domains. VisDA consists of a synthetic domain and two real-image domains containing the same 12 object categories. The training set of VisDA contains synthetic images generated from 3D CAD models and the validation set includes real images selected from COCO dataset [52]. In our experiments, we set the training set of VisDA as source domain and validation set as target domain. For each domain of VisDA, we randomly select 500 images from each class for training. For unsupervised methods, all samples in the source and target domains are used for training. For semi-supervised methods, since there are no label samples in the target domain, we only use the samples in the source domain for training. Note that, the target domain samples can be used for training by our proposed ATH_M method.

B. Experimental Setup

1) *Feature Extraction*: For CIFAR-10 dataset, each image is transformed to a 512-dimensional GIST [53] feature vector. For SUN397 dataset, each image is reshaped to a 1,600-dimensional feature vector. For Office Home,

we follow [17], [19] and each image is represented by a 4096-dimensional feature extracted by VGG-16 network [22], thereby providing a homogeneous feature space. For Caltech&Amazon, Amazon utilizes SURF features and each image is encoded by 800-bin histograms, while Caltech adopts deep features and each image is encoded by a 4096-dimensional CNN feature vector [54]. For VisDA, the source images are extracted by ResNet-50 network [23] (obtaining 2048-dimensional features) while the target images are extracted by VGG-16 network [22] (obtaining 4096-dimensional features).

2) *Dimensionality Reduction*: For HeSDR and HeCDR subtasks, existing hashing methods cannot be directly applied since the feature dimensions of source and target domains are misaligned. For comparison, we first perform dimensionality reduction and then take the aligned features as the inputs of comparison methods. Specifically, if the feature dimension of source domain is larger than that of target domain, PCA [55] dimensionality reduction is performed on source domain, and the number of reduced features is determined by the feature dimension of target domain. Otherwise, we perform dimensionality reduction on target domain. Note that, our methods do not require such a feature preprocessing, thus avoiding information loss caused by dimensionality reduction.

3) *Implementation Details*: The proposed ATH is implemented in MATLAB on a standard PC with Intel 2.20-GHz CPU and 128-GB RAM. For the comparison methods, we use their public codes and the parameter selection observes from the corresponding papers. Following the experimental settings in [17], [19], for each dataset, we pick up 500 samples from the target domain randomly as the query samples, and the rest images are used for training. The length of hash codes is selected from the range of $\{16, 32, 48, 64, 96, 128\}$. For each method, we simply set the number of nearest neighbors $\eta_k \in \{\eta_s, \eta_t\}$ to 10 and the number of iterations It_e is set to 10. For the parameters $\alpha_s, \alpha_t, \beta_s, \beta_t, \lambda$, we set them to $10^{-2}, 10^{-1}, 10^{-3}, 10^{-1}, 1$ for ATH_U, $10^{-1}, 10^{-1}, 10^3, 10^{-2}, 1$ for ATH_M, $10^{-2}, 1, 10^{-3}, 10^{-3}, 10^{-2}$ for ATH_K, and $10^{-3}, 10^{-1}, 10^{-2}, 10^{-2}, 10^{-2}$ for ATH_S, respectively. To obtain stable results, we run 10 independent experiments for each method and the average value of 10 experiments is reported.

4) *Evaluation Protocol*: Following the settings in [17], we adopt the widely-used Mean Average Precision (MAP) as the evaluation metric and provide the precision-recall (PR) curves to evaluate the performance of different methods. Besides, we

³<http://www.cs.toronto.edu/~kriz/cifar.html>

TABLE IV
MAP (%) RESULTS OF DIFFERENT METHODS WITH VARYING CODE LENGTHS FROM 16 TO 128 ON THE HeSDR SUBTASK.

Method	16	32	48	64	96	128	16	32	48	64	96	128	16	32	48	64	96	128
	Am (4096d) → Ca (800d)						Ca (800d) → Am (4096d)						VisDA train (2048d) → validation (4096d)					
ITQ	21.40	25.02	25.95	26.60	27.04	27.51	53.69	61.02	62.30	61.85	60.48	59.69	44.19	49.88	49.17	49.82	50.25	50.33
SP	22.01	27.98	29.15	28.71	29.16	29.14	65.84	72.37	72.64	70.42	67.67	65.50	56.71	62.34	61.25	60.90	59.79	59.17
DPLM	17.92	21.60	21.44	23.79	23.30	24.15	60.78	69.05	72.81	75.27	76.06	78.03	55.67	64.68	69.56	70.61	71.34	71.81
SHSR	19.73	22.35	20.70	22.33	24.35	24.27	72.99	77.39	77.00	76.82	75.44	75.59	64.06	67.00	59.62	56.04	53.25	50.60
GTH	22.28	23.44	25.27	26.00	26.52	26.93	51.52	52.36	53.68	54.61	55.19	57.11	39.71	44.86	50.20	51.03	52.65	53.23
ATH_U	23.87	25.67	27.42	28.36	28.30	28.22	74.84	76.36	75.17	75.64	76.43	75.54	66.13	63.42	65.98	69.29	69.01	69.45

TABLE V
MAP (%) RESULTS OF DIFFERENT METHODS WITH VARYING CODE LENGTHS FROM 16 TO 128 ON THE HeCDR SUBTASK.

Method	16	32	48	64	96	128	16	32	48	64	96	128	16	32	48	64	96	128
	Am (4096d) → Ca (800d)						Ca (800d) → Am (4096d)						VisDA train (2048d) → validation (4096d)					
ITQ	9.76	10.10	9.86	9.92	9.78	9.79	9.24	9.72	9.71	9.78	9.80	9.83	8.23	7.90	8.10	7.99	8.25	8.31
SP	9.93	9.72	9.64	9.60	9.79	9.78	9.21	9.60	9.66	9.61	9.63	9.73	8.12	8.14	8.05	7.94	7.86	7.95
DPLM	9.61	9.96	9.91	9.61	10.14	9.88	10.30	10.48	10.37	10.15	9.78	9.98	8.59	8.90	8.49	8.14	9.08	7.94
SHSR	9.76	9.96	9.62	9.98	9.91	9.91	9.93	9.86	10.12	10.33	9.74	9.93	8.89	8.13	8.54	8.39	8.24	8.47
GTH	9.70	9.65	9.71	9.74	9.67	9.61	9.45	9.33	9.56	9.40	9.57	9.61	7.72	7.92	8.08	8.09	8.16	8.02
ATH_U	12.21	13.14	13.84	13.85	13.02	12.08	15.45	15.77	18.57	18.01	20.45	15.92	12.58	11.22	12.16	15.89	13.46	13.46

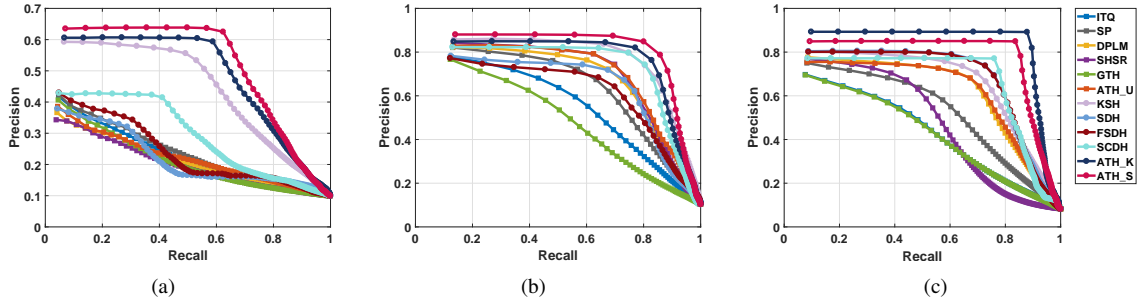


Fig. 5. PR curves on the HeSDR subtask. (a) Amazon → Caltech, (b) Caltech → Amazon, (c) VisDa train → validation.

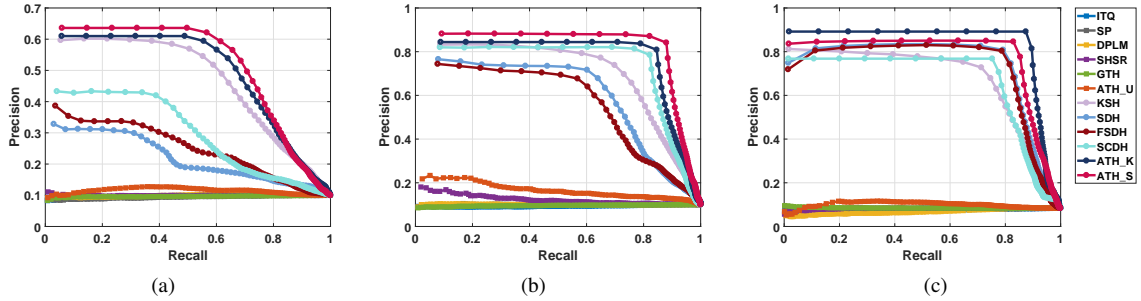


Fig. 6. PR curves on the HeCDR subtask. (a) Amazon → Caltech, (b) Caltech → Amazon, (c) VisDa train → validation.

also provide feature visualizations to illustrate the performance differences between different methods.

C. Performance on single-domain datasets

Table I provides the MAP results of unsupervised hashing methods on the single-domain benchmarks (the highest and second highest are marked in red and blue respectively). As we can see, the similarity-preservation based methods (i.e., DPLM, SHSR, ATH_U) always achieve better performance than the projection-based (i.e., ITQ, SP, GTH) methods in the single-domain setting, which stresses the importance to preserve the similarity relationship between pairwise samples. Moreover, although the proposed ATH_U is tailored for transfer retrieval, it can also outperform the traditional hashing

methods on the single-domain benchmarks. The potential reason is that the proposed ATH_U can adaptively learn the similarity relationship between samples from the data during the training stage.

D. Performance on cross-domain datasets

Tables II-V list the MAP results of unsupervised methods under four different GTR subtasks. Figures 3-6 provide the PR curves (with 64 bits) of all unsupervised and supervised methods under different GTR subtasks. As we can see, the proposed ATH_U obtains the best performance under different settings (i.e., HoSDR, HoCDR, HeSDR and HeCDR) in most cases, which demonstrates the effectiveness and versatility of our ATH framework for different GTR subtasks. Moreover,

TABLE VI
MAP (%) RESULTS OF SUPERVISED METHODS WITH 64BITS ON DIFFERENT GITR SUBTASKS.

Method	HoSDR			HoCDR			HeSDR			HeCDR		
	P→A	R→C	P→C	C→A	A→P	C→P	Am → Ca	Ca → Am	VisDA	Am → Ca	Ca → Am	VisDA
KSH	64.33	44.83	41.63	49.59	51.78	58.59	53.46	87.77	77.38	60.50	76.64	79.79
SDH	62.45	50.81	47.32	55.04	44.20	66.33	27.10	82.39	79.12	34.68	69.20	86.05
FSDH	66.61	55.66	51.83	59.14	73.27	70.85	32.75	77.44	78.54	41.55	64.39	84.75
SCDH	67.23	65.23	57.37	59.14	81.36	81.54	45.42	89.45	82.42	45.81	88.13	82.51
ATH_K	77.33	68.46	64.76	62.10	90.23	83.10	66.87	92.09	89.40	67.51	91.62	89.47
ATH_S	77.40	69.08	67.72	65.99	91.32	86.65	69.08	93.04	90.15	70.00	92.52	89.88

TABLE VII
MAP (%) RESULTS OF SEMI-SUPERVISED METHODS WITH 64BITS ON THE HOCDR SUBTASK.

Method	P→R	R→P	C→R	R→C	A→R	R→A
KSH	32.02	34.42	21.56	18.51	25.87	20.04
SDH	25.75	27.90	15.97	16.72	32.06	22.79
PWCF	34.03	34.44	24.22	18.42	34.57	28.95
DHLing	48.47	45.24	30.81	25.15	43.30	38.68
ATH_M	50.69	52.16	33.79	29.14	50.97	42.80

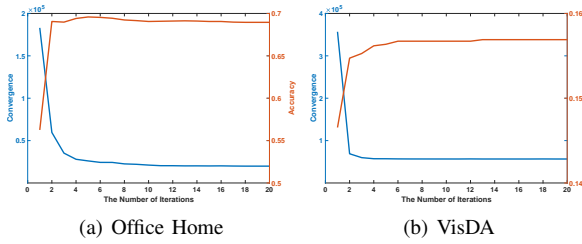


Fig. 7. Accuracy and convergence curves on different datasets.

we observe that the compared unsupervised methods are as effective as the proposed ATH_U on HeSDR subtask, but their performances are worse than that of ATH_U on HeCDR subtask. This is because the features and domains of query and retrieval sets in HeCDR subtask are misaligned and different. By simultaneously learning asymmetric hash functions and affinity relationship of cross-domain data, our method can perform knowledge transfer between domains and avoid information loss caused by feature alignment.

In addition, Table VI lists the MAP results of supervised methods under different GITR subtasks and VII provides the MAP results of different methods in the semi-supervised setting. Since the source code of DHLing is not publicly available, we directly cite the results of DHLing with 64bits using the same experimental settings with ours. From the experimental results, we observe that our ATH_M, ATH_S and ATH_K method obtain better retrieval performance than the state-of-the-art hashing methods. The reason is that our methods can perform positive transfer during training, as illustrated in the next section.

E. Positive Transfer or Not

We take ATH_M as an example to study whether the proposed ATH framework can achieve positive transfer or not. Firstly, we use a KNN model ($k = 1$) trained on labeled source domain to classify the unlabeled target domain data. In each iteration ite , the pseudo-labels $\tilde{\mathbf{Y}}_t^{ite}$ of target domain samples

TABLE VIII
MAP (%) RESULTS OF VARIANTS OF ATH_U (WITH 64 BITS).

Variants	HoSDR	HoCDR	HeSDR	HeCDR
	P→R	A→C	Ca → Am	VisDA
$\mathcal{T}_1 + \mathcal{T}_2$	44.62	17.11	58.09	9.67
$\mathcal{T}_1 + \mathcal{T}_3$	47.54	18.65	66.71	13.69
ATH_U	51.70	21.75	75.64	15.89

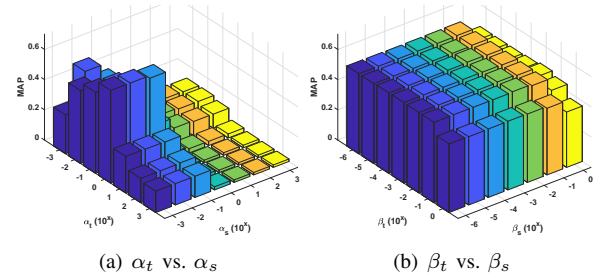


Fig. 8. Parameter sensitivity on A → C task.

are obtained by:

$$\tilde{\mathbf{Y}}_t^{ite+1} = \text{KNN}(\mathbf{A}_t^{Tite} \mathbf{X}_t, \mathbf{A}_s^{Tite} \mathbf{X}_s, \mathbf{Y}_s). \quad (30)$$

For initial $\tilde{\mathbf{Y}}_t^1$, we set

$$\tilde{\mathbf{Y}}_t^1 = \begin{cases} \text{KNN}(\mathbf{X}_t, \mathbf{X}_s, \mathbf{Y}_s), & \text{if homogeneous,} \\ \text{KNN}(\mathbf{A}_{t,pca}^T \mathbf{X}_t, \mathbf{A}_{s,pca}^T \mathbf{X}_s, \mathbf{Y}_s), & \text{otherwise.} \end{cases} \quad (31)$$

where $\mathbf{A}_{t,pca}$ and $\mathbf{A}_{s,pca}$ are initialized by PCA projections. Then, in each iteration ite , the classification accuracy $Accuracy^{ite}$ with respect to pseudo-labels $\tilde{\mathbf{Y}}_t^{ite}$ on target domain can be calculated by:

$$Accuracy^{ite} = \frac{\sum_j^{n_t} \mathcal{I}(\tilde{\mathbf{Y}}_{t,j}^{ite}, \mathbf{Y}_{t,j})}{n_t}, \quad (32)$$

where $\mathbf{Y}_{t,j}$ is the j -th column of \mathbf{Y}_t , $\mathcal{I}(a, b)$ is an indicator function, if vector a equals to b , $\mathcal{I}(a, b) = 1$, otherwise, $\mathcal{I}(a, b) = 0$. Figure 7 shows the accuracy and convergence curves of the proposed ATH_M on homogeneous ($A \rightarrow P$) and heterogeneous (VisDA train → validation) tasks. As we can see, our designed optimization algorithm converges fast. Moreover, with the increase of iteration times, the accuracy gradually increases and finally reaches stability, which demonstrates the validity of the mapping space learned by the proposed ATH_M. Therefore, our ATH_M can achieve positive transfer during the training process, which is a potential reason that why our methods outperform the other comparison methods on different GITR subtasks.

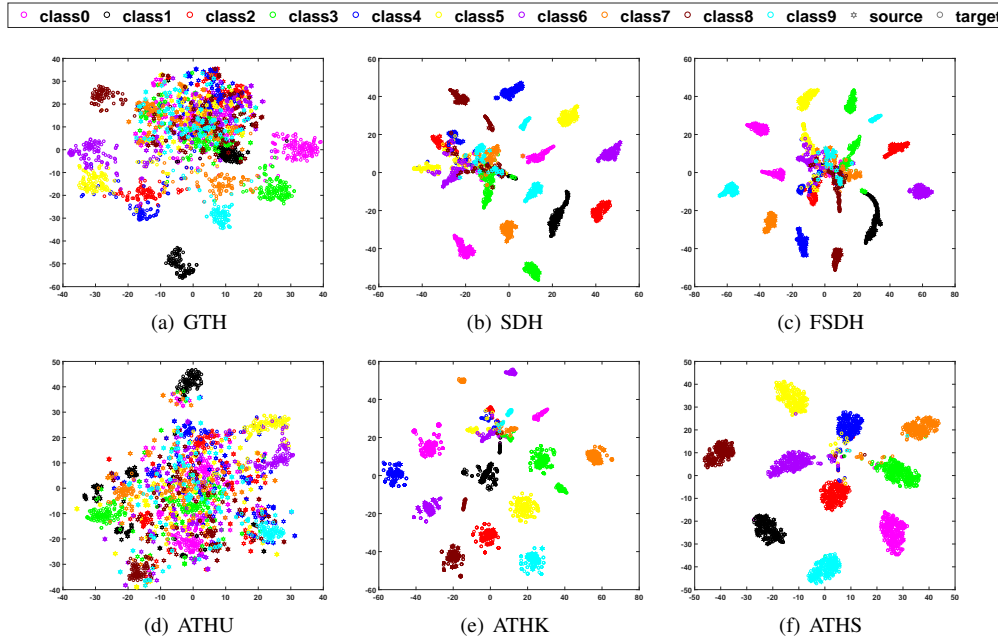


Fig. 9. Feature visualizations of different methods on the Caltech \rightarrow Amazon task.

F. Parameter Sensitivity

Figure 8 shows the parameter sensitivity of the proposed ATH_S on Office Home A \rightarrow C task. In this experiment, we fix $\lambda = 10^{-2}$ and $r = 16$. From Figure 8, we observe that the performance of ATH_S is relatively stable to β_k in the range of $[10^{-6}, 10^{-1}]$. However, α_k affects the MAP scores of ATH_S to a great extent. Specifically, ATH_S can work well when α_s and α_t are in the ranges of $[10^{-3}, 10^{-1}]$ and $[10^{-2}, 10^0]$, respectively.

G. Ablation Study

Table VIII lists ablation experimental results of the proposed ATH_U. Obviously, ATH_U obtains better performance under different GITH subtasks, which indicates the effectiveness of each component of ATH_U. Moreover, without preserving domain structure (i.e., \mathcal{T}_3), the MAP values of ATH_U will decrease significantly in most cases, which demonstrates the necessity of maintaining the intrinsic geometrical structure of data in their respective domains.

H. Visualization

Figure 9 shows t-SNE visualizations [56] learned by GTH, SDH, FSDH, ATH_U, ATH_K and ATH_S on heterogeneous Caltech \rightarrow Amazon task, where the hexagon and circle points indicate the projected data from source and target domains respectively. As we can see, without semantic information, GTH and ATH_U cannot obtain distinct class structure. For SDH and FSDH, due to feature heterogeneity of data and information loss caused by dimensionality reduction, massive points of different classes are mixed together and hard to distinguish. More importantly, our ATH_K and ATH_S can make the source data of each class close to the target data of the same class, and far away from the data of different classes in both two domains.

VI. CONCLUSION

This paper presents a more difficult image transfer retrieval problem named GITH, which makes no restriction on the domains and feature spaces of query and retrieval sets. To solve the GITH problem, we propose an ATH framework with its unsupervised/semi-supervised/supervised realizations, based on asymmetric hashing strategy and adaptive bipartite graph learning. Extensive experiments conducted on different GITH subtasks and label settings demonstrate the effectiveness of our ATH framework. A potential limitation of the proposed ATH is that the class space of target domain needs to be aligned with that of source domain. For the class space misaligned problem, a possible solution is to integrate zero-shot learning approach into the proposed model, which is a potential research direction for our future work.

REFERENCES

- [1] J. Wang, T. Zhang, J. Song, N. Sebe, and H. T. Shen, "A survey on learning to hash," *IEEE Transactions on Pattern Analysis and Machine Intelligence*, vol. 40, no. 4, pp. 769–790, 2018.
- [2] Z. Zhang, G. Xie, Y. Li, S. Li, and Z. Huang, "SADIH: semantic-aware discrete hashing," in *AAAI Conference on Artificial Intelligence*, 2019, pp. 5853–5860.
- [3] X. Zhou, F. Shen, L. Liu, W. Liu, L. Nie, Y. Yang, and H. T. Shen, "Graph convolutional network hashing," *IEEE Transactions on Cybernetics*, vol. 50, no. 4, pp. 1460–1472, 2020.
- [4] S. He, B. Wang, Z. Wang, Y. Yang, F. Shen, Z. Huang, and H. T. Shen, "Bidirectional discrete matrix factorization hashing for image search," *IEEE Transactions on Cybernetics*, vol. 50, no. 9, pp. 4157–4168, 2020.
- [5] L. Liu, M. Yu, and L. Shao, "Unsupervised local feature hashing for image similarity search," *IEEE Transactions on Cybernetics*, vol. 46, no. 11, pp. 2548–2558, 2016.
- [6] Y. Chen, Z. Lai, Y. Ding, K. Lin, and W. Wong, "Deep supervised hashing with anchor graph," in *International Conference on Computer Vision*, 2019, pp. 9795–9803.
- [7] Z. Lai, Y. Chen, J. Wu, W. K. Wong, and F. Shen, "Jointly sparse hashing for image retrieval," *IEEE Transactions on Image Processing*, vol. 27, no. 12, pp. 6147–6158, 2018.

- [8] Z. Zhang, L. Liu, F. Shen, H. Shen, and L. Shao, "Binary multi-view clustering," *IEEE Transactions on Pattern Analysis and Machine Intelligence*, vol. 41, no. 7, pp. 1774–1782, 2019.
- [9] Z. Zhang, Z. Lai, Z. Huang, W. K. Wong, G. Xie, L. Liu, and L. Shao, "Scalable supervised asymmetric hashing with semantic and latent factor embedding," *IEEE Transactions on Image Processing*, vol. 28, no. 10, pp. 4803–4818, 2019.
- [10] C. Da, G. Meng, S. Xiang, K. Ding, S. Xu, Q. Yang, and C. Pan, "Nonlinear asymmetric multi-valued hashing," *IEEE Transactions on Pattern Analysis and Machine Intelligence*, vol. 41, no. 11, pp. 2660–2676, 2019.
- [11] J. T. Zhou, H. Zhao, X. Peng, M. Fang, Z. Qin, and R. S. M. Goh, "Transfer hashing: From shallow to deep," *IEEE Transactions on Neural Networks and Learning Systems*, vol. 29, no. 12, pp. 6191–6201, 2018.
- [12] S. J. Pan, I. W. Tsang, J. T. Kwok, and Q. Yang, "Domain adaptation via transfer component analysis," *IEEE Transactions on Neural Networks*, vol. 22, no. 2, pp. 199–210, 2011.
- [13] M. Jing, J. Zhao, J. Li, L. Zhu, Y. Yang, and H. T. Shen, "Adaptive component embedding for domain adaptation," *IEEE Transactions on Cybernetics*, vol. 51, no. 7, pp. 3390–3403, 2021.
- [14] B. H. Nguyen, B. Xue, P. Andrae, and M. Zhang, "A hybrid evolutionary computation approach to inducing transfer classifiers for domain adaptation," *IEEE Transactions on Cybernetics*, vol. 51, no. 12, pp. 6319–6332, 2021.
- [15] Z. Cao, M. Long, C. Huang, and J. Wang, "Transfer adversarial hashing for hamming space retrieval," in *AAAI Conference on Artificial Intelligence*, 2018, pp. 6698–6705.
- [16] L. Zhang, J. Liu, Y. Yang, F. Huang, F. Nie, and D. Zhang, "Optimal projection guided transfer hashing for image retrieval," *IEEE TCSVT*, vol. 30, no. 10, pp. 3788–3802, 2020.
- [17] F. Huang, L. Zhang, Y. Yang, and X. Zhou, "Probability weighted compact feature for domain adaptive retrieval," in *International Conference on Computer Vision and Pattern Recognition*, 2020, pp. 9579–9588.
- [18] F. Huang, L. Zhang, and X. Gao, "Domain adaptation preconceived hashing for unconstrained visual retrieval," *IEEE Transactions on Neural Networks and Learning Systems*, pp. 1–15, 2021.
- [19] H. Xia, T. Jing, C. Chen, and Z. Ding, "Semi-supervised domain adaptive retrieval via discriminative hashing learning," in *ACM International Conference on Multimedia*. ACM, 2021, pp. 3853–3861.
- [20] M. J. Swain and D. H. Ballard, "Indexing via color histograms," in *International Conference on Computer Vision*, 1990, pp. 390–393.
- [21] D. G. Lowe, "Distinctive image features from scale-invariant keypoints," *International Journal of Computer Vision*, vol. 60, no. 2, pp. 91–110, 2004.
- [22] K. Simonyan and A. Zisserman, "Very deep convolutional networks for large-scale image recognition," in *International Conference on Learning Representations*, 2015.
- [23] K. He, X. Zhang, S. Ren, and J. Sun, "Deep residual learning for image recognition," in *International Conference on Computer Vision and Pattern Recognition*, 2016, pp. 770–778.
- [24] A. Gordo, F. Perronnin, Y. Gong, and S. Lazebnik, "Asymmetric distances for binary embeddings," *IEEE Transactions on Pattern Analysis and Machine Intelligence*, vol. 36, no. 1, pp. 33–47, 2014.
- [25] W. Dong, M. Charikar, and K. Li, "Asymmetric distance estimation with sketches for similarity search in high-dimensional spaces," in *Annual International ACM SIGIR Conference on Research and Development in Information Retrieval*, 2008, pp. 123–130.
- [26] B. Neyshabur, N. Srebro, R. R. Salakhutdinov, Y. Makarychev, and P. Yadollahpour, "The power of asymmetry in binary hashing," in *Advances in Neural Information Processing Systems*, 2013, pp. 2823–2831.
- [27] Y. Luo, Y. Li, F. Shen, Y. Yang, P. Cui, and Z. Huang, "Collaborative learning for extremely low bit asymmetric hashing," *IEEE Transactions on Knowledge and Data Engineering*, 2020.
- [28] F. Shen, X. Gao, L. Liu, Y. Yang, and H. T. Shen, "Deep asymmetric pairwise hashing," in *ACM International Conference on Multimedia*, 2017, pp. 1522–1530.
- [29] Q. Jiang and W. Li, "Asymmetric deep supervised hashing," in *AAAI Conference on Artificial Intelligence*, 2018, pp. 3342–3349.
- [30] A. Iscen, G. Tolias, Y. Avrithis, T. Furon, and O. Chum, "Efficient diffusion on region manifolds: Recovering small objects with compact CNN representations," in *International Conference on Computer Vision and Pattern Recognition*, 2017, pp. 926–935.
- [31] C. Liu, G. W. Yu, M. Volkovs, C. Chang, H. Rai, J. Ma, and S. K. Gorti, "Guided similarity separation for image retrieval," in *Advances in Neural Information Processing Systems*, 2019, pp. 1554–1564.
- [32] C. Zhang and W. Zheng, "Semi-supervised multi-view discrete hashing for fast image search," *IEEE Transactions on Image Processing*, vol. 26, no. 6, pp. 2604–2617, 2017.
- [33] X. Fang, Y. Xu, X. Li, Z. Lai, W. K. Wong, and B. Fang, "Regularized label relaxation linear regression," *IEEE Transactions on Neural Networks and Learning Systems*, vol. 29, no. 4, pp. 1006–1018, 2018.
- [34] X. Guo, "Robust subspace segmentation by simultaneously learning data representations and their affinity matrix," in *International Joint Conference on Artificial Intelligence*, 2015, pp. 3547–3553.
- [35] C. Li, L. Lin, W. Zuo, J. Tang, and M. Yang, "Visual tracking via dynamic graph learning," *IEEE Transactions on Pattern Analysis and Machine Intelligence*, vol. 41, no. 11, pp. 2770–2782, 2019.
- [36] Y. Luo, Z. Huang, Z. Wang, Z. Zhang, and M. Baktashmotlagh, "Adversarial bipartite graph learning for video domain adaptation," in *ACM International Conference on Multimedia*. ACM, 2020, pp. 19–27.
- [37] J. Wen, Z. Zhang, Z. Zhang, L. Fei, and M. Wang, "Generalized incomplete multiview clustering with flexible locality structure diffusion," *IEEE Transactions on Cybernetics*, vol. 51, no. 1, pp. 101–114, 2021.
- [38] F. Shen, C. Shen, W. Liu, and H. Shen, "Supervised discrete hashing," in *International Conference on Computer Vision and Pattern Recognition*, 2015, pp. 37–45.
- [39] W. Liu, J. Wang, S. Kumar, and S. Chang, "Hashing with graphs," in *International Conference on Machine Learning*, 2011, pp. 1–8.
- [40] Z. Lai, Y. Chen, J. Wu, W. K. Wong, and F. Shen, "Jointly sparse hashing for image retrieval," *IEEE Transactions on Image Processing*, vol. 27, no. 12, pp. 6147–6158, 2018.
- [41] Y. Gong, S. Lazebnik, A. Gordo, and F. Perronnin, "Iterative quantization: A procrustean approach to learning binary codes for large-scale image retrieval," *IEEE Transactions on Pattern Analysis and Machine Intelligence*, vol. 35, no. 12, pp. 2916–2929, 2013.
- [42] Y. Xia, K. He, P. Kohli, and J. Sun, "Sparse projections for high-dimensional binary codes," in *International Conference on Computer Vision and Pattern Recognition*, 2015, pp. 3332–3339.
- [43] F. Shen, X. Zhou, Y. Yang, J. Song, H. T. Shen, and D. Tao, "A fast optimization method for general binary code learning," *IEEE Transactions on Image Processing*, vol. 25, no. 12, pp. 5610–5621, 2016.
- [44] D. Hu, F. Nie, and X. Li, "Discrete spectral hashing for efficient similarity retrieval," *IEEE Transactions on Image Processing*, vol. 28, no. 3, pp. 1080–1091, 2019.
- [45] W. Liu, J. Wang, R. Ji, Y. Jiang, and S. Chang, "Supervised hashing with kernels," in *International Conference on Computer Vision and Pattern Recognition*, 2012, pp. 2074–2081.
- [46] J. Gui, T. Liu, Z. Sun, D. Tao, and T. Tan, "Fast supervised discrete hashing," *IEEE Transactions on Pattern Analysis and Machine Intelligence*, vol. 40, no. 2, pp. 490–496, 2018.
- [47] Y. Chen, Z. Tian, H. Zhang, J. Wang, and D. Zhang, "Strongly constrained discrete hashing," *IEEE Transactions on Image Processing*, vol. 29, pp. 3596–3611, 2020.
- [48] J. Xiao, J. Hays, K. A. Ehinger, A. Oliva, and A. Torralba, "SUN database: Large-scale scene recognition from abbey to zoo," in *IEEE Conference on Computer Vision and Pattern Recognition*, 2010, pp. 3485–3492.
- [49] H. Venkateswara, J. Eusebio, S. Chakraborty, and S. Panchanathan, "Deep hashing network for unsupervised domain adaptation," in *International Conference on Computer Vision and Pattern Recognition*, 2017, pp. 5385–5394.
- [50] B. Gong, Y. Shi, F. Sha, and K. Grauman, "Geodesic flow kernel for unsupervised domain adaptation," in *International Conference on Computer Vision and Pattern Recognition*, 2012, pp. 2066–2073.
- [51] X. Peng, B. Usman, K. Saito, N. Kaushik, J. Hoffman, and K. Saenko, "Syn2Real: A new benchmark for synthetic-to-real visual domain adaptation," *CoRR*, vol. abs/1806.09755, 2018.
- [52] T. Lin, M. Maire, S. J. Belongie, J. Hays, P. Perona, D. Ramanan, P. Dollár, and C. L. Zitnick, "Microsoft COCO: common objects in context," in *European Conference on Computer Vision*, 2014, pp. 740–755.
- [53] A. Oliva and A. Torralba, "Modeling the shape of the scene: A holistic representation of the spatial envelope," *International Journal of Computer Vision*, vol. 42, no. 3, pp. 145–175, 2001.
- [54] J. Donahue, Y. Jia, O. Vinyals, J. Hoffman, N. Zhang, E. Tzeng, and T. Darrell, "Decaf: A deep convolutional activation feature for generic visual recognition," in *International Conference on Machine Learning*, 2014, pp. 647–655.
- [55] M. A. Turk and A. Pentland, "Face recognition using eigenfaces," in *International Conference on Computer Vision and Pattern Recognition*, 1991, pp. 586–591.

- [56] V. D. M. Laurens and G. Hinton, “Visualizing data using t-sne,” *Journal of Machine Learning Research*, vol. 9, no. 2605, pp. 2579–2605, 2008.